Tampere University

Niklas Järvelin

THE COLLECTIVE OPTICAL RESPONSES OF PERIODIC HOLE ARRAYS IN METALLIC FILMS

A comparison with nanoparticle arrays

Bachelor thesis
Faculty of Engineering and Natural Sciences
Examiners: Mikko J. Huttunen
Madona Mekhael
May 2023

ABSTRACT

Niklas Järvelin: The collective optical responses of periodic hole arrays in metallic films
Bachelor thesis
Tampere University
Engineering and Natural Sciences
May 2023

Metamaterials are artificial materials exhibiting nanoscale features with sizes of the order of the wavelength of incident light. These features change the optical properties of the material. One much-researched type of metamaterial is the metallic nanoparticle array. Nanoparticle arrays can exhibit two different types of resonances, those being the localized surface plasmon resonances (LSPRs) and the surface lattice resonances (SLRs). LSPRs are resonances inherent to a single particle or hole and SLRs are collective resonances of the whole lattice. These resonances are utilized in many different applications in photonics. Interestingly, the complementary structures of metallic nanoparticle arrays, hole arrays in metallic films can also exhibit these resonances.

The aim of this thesis is to research the collective optical responses of hole arrays and see how they compare to the collective optical responses of nanoparticle arrays. In particular, we study SLRs since their properties can be easily modified by changing lattice parameters. In the theory section of this thesis, we go through some general theory regarding particle arrays and hole arrays, in the methods section we introduce COMSOL Multiphysics simulation software and in the result section, we study the similarities and differences between particle arrays and hole arrays. We also study how to affect at which wavelengths the SLR occurs.

In this thesis, we observe that hole arrays have two different SLR peaks, unlike particle arrays which only have one. We also note that the less visible peak exhibits a significantly higher quality factor (Q-factor) values than the more visible SLR peak of the hole array or the SLR peak of the corresponding particle array. We study how the Q-factor and the SLR wavelength of the smaller peak depend on the thickness of the metallic film and show that the Q-factor increases and the SLR wavelength shortens as the metallic film gets thinner. This is opposite to what happens to the more visible SLR peak. Its Q-factor decreases and the SLR wavelength increases with thinner films. However, the SLR peak of particle arrays does not significantly change when we vary the height of the particle. We also studied how changing the periodicity of the hole array moves the SLR peak.

We managed to modify the collective optical responses of hole arrays by changing the thickness of the film and the length of the period. This enables their use in many applications of photonics that traditionally utilize particle arrays. Hole arrays also have advantages over particle arrays such as thermal conductivity. This enables using higher intensity lasers with metamaterials which could enable their use in novel applications.

Keywords: metamaterial, metasurface, nanoparticle array, hole array, aperture array, surface lattice resonance, SLR

TIIVISTELMÄ

Niklas Järvelin: Metallikalvoaukkohilojen kollektiiviset optiset vasteet
Kandidaatintyö
Tampereen yliopisto
Tekniikka ja luonnontieteet
Toukokuu 2023

Metamateriaalit ovat keinotekoisia materiaaleja, joissa on kokoluokaltaan valon aallonpituuden kokoisia rakenteita. Yksi paljon tutkittu metamateriaalien tyyppi on metalliset nanopartikkelihilat. Niissä on havaittu ilmenevän kahdenlaisia resonansseja, jotka ovat yksittäisiin partikkeleihin liittyvät paikalliset pintaplasmoniresonanssit (engl. Localized Surface Plasmon Resonance, LSPR) ja usean partikkelin kytkeytymiseen liittyvät pintahilaresonanssit (engl. Surface Lattice Resonance, SLR). Näitä resonansseja hyödynnetään monissa fotoniikan sovelluksissa. Partikkelihilat eivät kuitenkaan ole ainoita rakenteita, joissa näitä resonansseja esiintyy, sillä niitä ilmenee myös muun muassa metallisten partikkelihilojen vähemmän tutkituissa komplementtirakenteissa, metallikalvoaukkohiloissa.

Työn tavoite on tutkia metallikalvoaukkohilojen kollektiivisia optisia vasteita ja verrata niitä metallisten nanopartikkelihilojen optisiin vasteisiin. Huomiota kiinnitetään etenkin pintahilaresonansseihin, koska niiden ominaisuuksia voidaan helposti muokata muuttamalla hilan parametreja. Työn teoriaosuudessa käydään läpi nanopartikkelihilojen ja aukkohilojen yleistä teoriaa, menetelmäosuudessa kerrotaan COMSOL Multiphysics -simulaatio-ohjelmistosta ja tulososuudessa tutkitaan, millaisia yhtäläisyyksiä ja eroavaisuuksia aukkohilojen ja partikkelihilojen vasteissa on. Työssä tutkitaan myös, miten aukkohilojen SLR-aallonpituuksiin voidaan vaikuttaa.

Työssä havaitaan, että aukkohiloilla on kaksi eri SLR-piikkiä toisin kuin partikkelihiloilla, joilla on vain yksi. Toisella näistä piikeistä on huomattavasti suurempi Q-tekijä eli hyvyysluku kuin partikkelihilan SLR:llä tai aukkohilan toisella SLR:llä. Tämän piikin hyvyysluvun ja aallonpituuden riippuvuuksia metallikalvon paksuuteen tutkitaan ja osoitetaan, että hyvyysluku kasvaa ja aallonpituus lyhenee ohuemmilla kalvoilla. Tämä on päinvastoin kuin aukkohilojen toisella SLR-piikillä, jonka hyvyysluku pienenee ja aallonpituus suurenee ohuemmilla kalvoilla. Partikkelihiloissa sen sijaan partikkelien korkeuden muuttaminen ei vaikuta SLR-piikkeihin yhtä merkittävästi. Myös jaksollisuuden merkitystä aukkohilojen SLR-aallonpituuteen tutkitaan.

Aukkohilojen kollektiivisia optisia vasteita onnistuttiin muokkaamaan muuttamalla kalvon paksuutta ja hilan periodisuutta. Tämän perusteella aukkohilarakenteita voitaisiin mahdollisesti käyttää monissa fotoniikan sovelluksissa, joissa on perinteisesti käytetty partikkelihiloja. Aukkohiloille on myös vahvuuksia, kuten niiden suuri lämmönjohtokyky, joka mahdollistaa suurempien tehojen laserien käyttämistä metamateriaalien kanssa, ja tämä voi mahdollistaa myös aivan uudenlaisia sovelluskohteita.

Avainsanat: metamateriaali, metapinta, nanopartikkelihila, aukkohila, pintahilaresonanssi, SLR

CONTENTS

LIST OF SYMBOLS AND ABBREVIATIONS

α_{E}	electric polarizability
α_{M}	magnetic polarizability
e	elementary charge
e	Euler's number
$\mathbf{E}^{\mathrm{ext}}$	external electric field
$\mathbf{E}_x$	electric field component in the x-direction
$\mathbf{E}_y$	electric field component in the y-direction
$\mathbf{E}_z$	electric field component in the z-direction
ε_0	vacuum permittivity
ε_∞	relative permittivity at high frequencies
ε_{r}	relative permittivity
G	lattice sum
$\mathcal{G}^0$	dipole–dipole interaction tensor
γ	characteristic collision frequency
$\mathbf{H}^{\mathrm{ext}}$	external magnetic field
$\mathbf{H}_x$	magnetic field component in the x-direction
$\mathbf{H}_y$	magnetic field component in the y-direction
$\mathbf{H}_z$	magnetic field component in the z-direction
i	Cartesian coordinate index
i	imaginary unit
j	Cartesian coordinate index
k	wave number
$\mathbf{k}_{\|\|}$	wave vector parallel to the surface
λ_0	wavelength of a peak
$\lambda_{i,j}$	Rayleigh anomaly wavelength
λ_x	wavelength of the first-order Rayleigh anomaly of x-polarized light
$\Delta\lambda$	line width of a peak

LSPR	Localized Surface Plasmon Resonance
$\mathbf{m}$	magnetic dipole moment
m	effective optical mass of an electron
n	index
n	refractive index
n_f	number density of free electrons
ω	angular frequency
ω_p	plasma frequency
$\mathbf{p}$	electric dipole moment
p_x	period to the x-direction
p_y	period to the y-direction
ϕ	azimuthal angle
Q	quality factor
r	distance
$\mathbf{r}$	position
$\mathbf{R}_n$	position of the nth nanoparticle
SLR	Surface Lattice Resonance
SPP	Surface Plasmon Polariton
TE	Transverse Electric
TM	Transverse Magnetic
θ	polar angle
x	in-plane Cartesian coordinate
y	in-plane Cartesian coordinate
z	Cartesian coordinate normal to the plane

1. INTRODUCTION

In recent years there has been a lot of interest regarding metamaterials, artificial materials exhibiting nanoscale features with sizes of the order of the wavelength of incident light. When all the features of a metamaterial are positioned along a single two-dimensional plane the structure is called a metasurface. The features of a metasurface change the optical properties of the material and can thus be used to control the optical properties of the material by changing the size and shape of the features. The features also affect the optical properties of the material collectively. The fields scattered from nearby features change the local field around a feature giving rise to collective responses. Controlling the optical properties is useful because it enables one to control the wavefronts of light, and this can be used in different kinds of applications ranging from holography [1, 2] to flat lenses [3, 4] to enhancing non-linear processes [5].

Much of this research has focused on metasurfaces composed of nanoparticles. These are materials that have small clusters of another material, usually metals or silicon-based compounds, in a uniform environment. This environment is usually some type of glass.

Despite many advantages of using nanoparticles, their use is not without problems. For example, when working with metallic nanopartivles the nanoparticles can considerably heat up when subjected to high-intensity light for long periods of time. Because it is expensive to to embed nanoparticles inside a medium which is both optically transparent and a good thermal conductor, the cooling of nanoparticles is a relatively slow process. Therefore, under intense conditions, the particles exhibit high ohmic losses and can even melt down damaging the material.

The complementary structures of nanoparticle arrays are called hole arrays. They are metallic films that have small holes in them. Hole arrays are also metasurfaces that can be used in similar manner to nanoparticle arrays. However, hole arrays have the advantage that heating is not a problem since the metasurface can also cool down by thermal conduction. This would enable the use of lasers with higher intensities without damaging the material thus enhancing non-linear optical processes even further.

In this thesis, we study the collective optical responses of periodic hole metasurfaces in metallic films and aim to find similarities and differences between those responses and the responses of nanoparticle metasurfaces. We aim to make it easier to design hole

arrays that have desired responses. This would enable us to use the advantages inherent in hole arrays such as increased heat resistance.

Chapter 2 introduces the optical properties of metals and the physics behind arrays of metallic nanoparticles. In Chapter 3 we introduce hole arrays in metallic films and compare them to nanoparticle arrays. Chapter 4 is an introduction to the COMSOL Multiphysics software which is used for the simulations of this thesis. The simulation results are shown in Chapter 5 where they are also analyzed.

2. PERIODIC ARRAYS OF METALLIC NANOPARTICLES

Nanoparticles, also known as meta-atoms or in metamaterial context simply as particles, are small clusters of some material whose dimensions are of the order of tens or hundreds of nanometers. Therefore, they are smaller than optical wavelengths. Nanoparticles are often made of metal but also silicon and its compounds are used. In this section, only metallic nanoparticles are discussed although a lot of the physics is similar to dielectric and semiconducting nanoparticles. The response of an individual metallic nanoparticle is first introduced after which the treatment is extended to an array of these particles.

2.1 The optical response of an individual metallic nanoparticle

The optical properties of metals can be explained by the Drude model, also sometimes known as the plasma model, introduced in S. Maier's book [6, pages 11–18]. Drude theory assumes that a metal consists of a gas of free electrons that can move and oscillate freely relative to the positive ion cores. The cores are assumed to be massive enough to not move at all. The Drude model does not take into account details of the lattice potential or electron–electron interactions. It also ignores interband transitions limiting its validity.

The relative permittivity $\varepsilon_{\mathrm{r}}(\omega)$ of a metal depends on the angular frequency of the incoming light ω and according to the Drude model is

$$\varepsilon_{\mathrm{r}}(\omega) = \varepsilon_{\infty} - \frac{\omega_{\mathrm{p}}^2}{\omega^2 + \mathrm{i}\gamma\omega} \tag{2.1}$$

where ε_{∞} is a constant characteristic to a metal, ω_{p} is the plasma frequency, i is the imaginary unit and γ is the characteristic collision frequency. The plasma frequency is a characteristic of a metal that is dependent on the number density of free electrons n_f and can be written as

$$\omega_{\mathrm{p}}^2 = \frac{n_f e^2}{\varepsilon_0 m} \tag{2.2}$$

where e is the elementary charge, ε_0 is the vacuum permittivity and m is the effective optical mass of an electron. This mass incorporates some effects of the band structure of the metal and therefore isn't the same for all metals. It is important to note that Eq. (2.2) gives the plasma frequency in a bulk metal. However, the effective plasma frequency is smaller in nanoparticles [7].

The Drude model assumes that there are electrons in a metal that can freely oscillate when subjected to an external electric field $\mathbf{E}^{\mathrm{ext}}$. This induces an electric dipole moment $\mathbf{p}$ in the nanoparticle [8]. The direction of the electric dipole moment is in the direction of the external electric field. The physial meaning of the electric dipole moment is that the nanoparticle is assumed to mostly radiate and scatter light like an electric dipole source. The direction of the electric dipole moment affects the direction where the dipole source radiates. If the incident electric field is x-polarized, the electric dipole moment is to the x-direction and therefore it does not radiate to the x-direction but it does radiate to the y-direction [9, page 73].

The electric dipole moment can be expressed using electric polarizability α_{E} as [8]

$$\mathbf{p} = \alpha_{\mathrm{E}} \mathbf{E}^{\mathrm{ext}} \tag{2.3}$$

In a general case, the electric polarizability is a 3 by 3 tensor that describes the behavior of the nanoparticle under an external electric field $\mathbf{E}^{\mathrm{ext}}$. Therefore, it is dependent on the size and shape of the nanoparticle. However, for the purposes of this thesis, the polarizability can be reduced to a scalar due to symmetries inherent in the studied nanoparticles.

Oscillating electrons in a metallic nanoparticle can also give rise to a new phenomenon. With certain frequencies of incoming light, this oscillating charge density can begin to resonate inside the nanoparticle in a phenomenon called localized surface plasmon resonance (LSPR). LSPRs are associated with large dipole moments. Therefore, LSPR frequencies are the frequencies where the polarizability is the largest.

LSPR is sensitive to the refractive index of the surrounding material and it enhances the local electric field [10]. Because of these effects, LSPRs can be used for many different applications. LSPRs also affect the transmission of a particle metasurface and the LSPR frequency can be detected as a wide peak in the transmission spectra.

2.2 Collective optical responses of metallic nanoparticle lattices

The optical response of a nanoparticle lattice differs from the optical response of an individual nanoparticle because the nanoparticles in an array can behave collectively. When there are multiple nanoparticles in an array they can couple with each other via dipole–dipole interactions. These interactions are dependent on the position vector $\mathbf{r}$ between the two coupled particles, and can be described by the dipole–dipole interaction tensor $\mathcal{G}^0(\mathbf{r})$. The dipole–dipole interaction tensor can be written as [8]

$$\mathcal{G}^0(\mathbf{r}) = (k^2 + \nabla\nabla)\frac{\mathrm{e}^{-\mathrm{i}kr}}{r} \tag{2.4}$$

where k is the wave number, ∇ is the differential operator, e is Euler's number and r is the norm of the position vector $\mathbf{r}$.

These interactions affect the dipole moments induced in the nanoparticles and therefore, in an array, Eq. (2.3) doesn't hold. However, an equation for the dipole moment of a nanoparticle can be derived for nanoparticles in an array. This equation is

$$\mathbf{p} = \frac{1}{1/\alpha_{\mathrm{E}} - G(\mathbf{k}_{||})}\mathbf{E}^{\mathrm{ext}} \tag{2.5}$$

where $G(\mathbf{k}_{||})$ is a correction term to the polarizability. It is the sum of all of the dipole–dipole interactions and can be written as

$$G(\mathbf{k}_{||}) = \sum_{n\neq 0} \mathcal{G}^0(\mathbf{R}_n)\mathrm{e}^{-\mathrm{i}\mathbf{k}_{||}\cdot\mathbf{R}_n} \tag{2.6}$$

where $\mathbf{R}_n$ is the position of a nanoparticle and $\mathbf{k}_{||}$ is the wave vector parallel to the surface. Also, $\mathbf{R}_0$ is defined to be a zero vector i.e. the particle whose dipole moment is being calculated is in the origin.

Arrays, which consist of tens of thousands of nanoparticles, can be approximated as infinite. When this approximation applies, $G(\mathbf{k}_{||})$ has the same value for all particles and therefore it only needs to be calculated once. The method of calculating the collective response of a nanoparticle array using this approximation and Eq. (2.5) is also known as the lattice-sum approach [11].

When the divider in Eq. (2.5) approaches zero a new resonance occurs [5, 12]. This resonance happens due to the periodic nature of the metasurface and is called surface lattice resonance (SLR). SLR is a collective resonance of the lattice and its frequency is therefore not only dependent on the properties of the nanoparticle, such as shape, size and material but also by the lattice properties like periodicity. The direction of the periodicity on which the SLR wavelength depends is the in-plane direction which is perpendicular to the polarization [13]. Like LSPRs, SLRs give rise to a peak in the transmission spectra. However, these peaks are much narrower than LSPR peaks and therefore they have much higher Q-factors meaning longer resonance lifetimes [5]. This makes them better for applications like enhancing non-linear optical effects.

For a deeper understanding of how the periodicity affects the SLR wavelength, it is useful to note that the SLR wavelength is related to Rayleigh anomalies (RAs) [5, 14]. The Rayleigh anomaly wavelengths $\lambda_{i,j}$ are given by the equation [5, 14]

$$\lambda_{i,j} = -A + \sqrt{A^2 - B} \tag{2.7}$$

where i and j are the diffraction orders along the Cartesian coordinates. A and B are

given by equations

$$A = \frac{\sin(\theta)}{(i/p_x)^2 + (j/p_y)^2} \left(\frac{i \sin(\phi)}{p_x} + \frac{j \cos(\phi)}{p_y} \right) \tag{2.8}$$

and

$$B = \frac{\sin^2(\theta) - n^2}{(i/p_x)^2 + (j/p_y)^2} \tag{2.9}$$

where θ is the polar angle, p_x and p_y are the periods along the Cartesian coordinates, ϕ is the azimuthal angle and n is the refractive index of the surrounding material. With x-polarized light $(\phi = 0°)$ and normal incidence $(\theta = 0°)$ the wavelength of the first-order SLR λ_x can be reduced to the form [5]

$$\lambda_x = p_y n \tag{2.10}$$

From this equation, we can conclude that the SLR wavelength for x-polarized light is directly proportional to the period in the y-direction. This is caused by the fact that the direction of the electric dipole moment of the nanoparticle doesn't allow the nanoparticle to radiate to the x-direction and therefore there is no way for the nanoparticles to couple in that direction.

3. PERIODIC HOLE ARRAYS IN METALLIC FILMS

A hole array, also known as an aperture array, is the complementary structure of a nanoparticle array. Instead of having metallic particles in a dielectric environment, a hole array is a metallic film in which there are holes filled with the dielectric substance. While particle arrays transmit light hole arrays reflect light. Because hole arrays are complementary structures to particle arrays, much of the physics already discussed in the particle array chapter have similar counterparts in hole arrays. As was the case in the particle array chapter, first we will formulate a treatment to understand the optical response of a single hole in a metallic film after which the treatment is extended hole arrays.

3.1 The optical response of an individual hole

Since holes are the complementary structure to nanoparticles, the optical responses of holes are related to the responses of nanoparticles through Babinet's principle. According to this principle the spatial distribution of the transmitted electric field in a nanoparticle array is the same as the spatial distribution of the reflected magnetic field in a hole array [15, 16]. However, the electric and magnetic in-plane polarizations are interchanged.

Babinet's principle holds perfectly for thin films of ideal metals [15]. For thicker films, its validity is more limited. In this thesis, the films are too thick relative to the wavelength of the incident light for Babinet's principle to give a valid quantitative approximation of the reflected field of a hole array. However, similarities between the transmission of a particle array and the reflectance of a hole array should be expected. It may also be noted that interband absorptions can also decrease the validity of Babinet's principle [15].

As was the case for nanoparticles, the external electric field $\mathbf{E}^{\mathrm{ext}}$ induces an electric dipole moment $\mathbf{p}$ in single holes. The equation for this is the same as for nanoparticles, that being the Eq. (2.3). This was described by Bethe in his 1944 paper [17]. The exact results of Bethe are beyond the scope of this thesis. Furthermore, Bethe's results are for thin films which somewhat limits their validity for the purposes of this thesis. However, an electric dipole moment is induced also in thick films [8].

The direction of the electric dipole moment in a hole differs from the direction of the electric dipole moment in a particle. As was said in Section 2.1, for nanoparticles the direction

of the dipole moment is in the direction of the polarization of incoming light of normal incidence. Therefore, the electric dipole moment is parallel to the surface. However, in holes there cannot be parallel electric dipole moments due to boundary conditions imposed by Maxwell's equations near dielectric–metal interfaces [8, 17, 18]. In fact, the electric dipole moment in holes points along the normal of the metasurface plane.

In addition to electric dipole moments, holes also exhibit magnetic dipole moments. The equation for these magnetic dipole moments $\mathbf{m}$ is [8]

$$\mathbf{m} = \alpha_{\mathrm{M}} \mathbf{H}^{\mathrm{ext}} \tag{3.1}$$

where α_{M} is the magnetic polarizability of the hole and $\mathbf{H}^{\mathrm{ext}}$ is the external magnetic field. The direction of a magnetic dipole moment in a hole is parallel to the metallic film and perpendicular to the polarization [8].

For the case of thicker metallic films, the optical response of individual holes cannot be accurately described by using a single dipole moment. Instead, a better approximation is to use two electric and two magnetic dipole moments, one on top of the hole and another at the bottom of the hole, to describe the response of the hole [8].

Differences in the dipole moments between an individual nanoparticle and an individual hole can be seen in Fig. 3.1. While a particle only has one electric dipole moment $\mathbf{p}$, the hole has two different electric and magnetic dipole moments on the top of the hole and at the bottom of the hole. Also, the direction of the electric dipole moment is different in a hole compared to a particle.

Like particles, holes also exhibit LSPRs [19]. In holes, the resonating localized surface plasmons are localized on the rim of the holes [20].

3.2 Propagating surface plasmons in metallic films

Like particle arrays, hole arrays also have collective optical responses. To understand these phenomena one must understand how holes can couple to one another. While particles can couple to each other simply by light, holes have metal between them through which light can't penetrate. Therefore, surface plasmons are needed for holes to couple.

Surface plasmon polaritons (SPPs) are electromagnetic excitations that propagate on the interface of a metal and a dielectric material [6]. SPPs arise via the coupling of light to the oscillations of the electrons of the metal.

Propagating electromagnetic waves can be split into two different modes, those being the transverse magnetic (TM) and the transverse electric (TE) modes [6]. However, only the TM mode is possible on the interface of a metal and a dielectric material [6]. Therefore, for an SPP propagating to the x-direction on a metallic film in the xy-plane the only possible

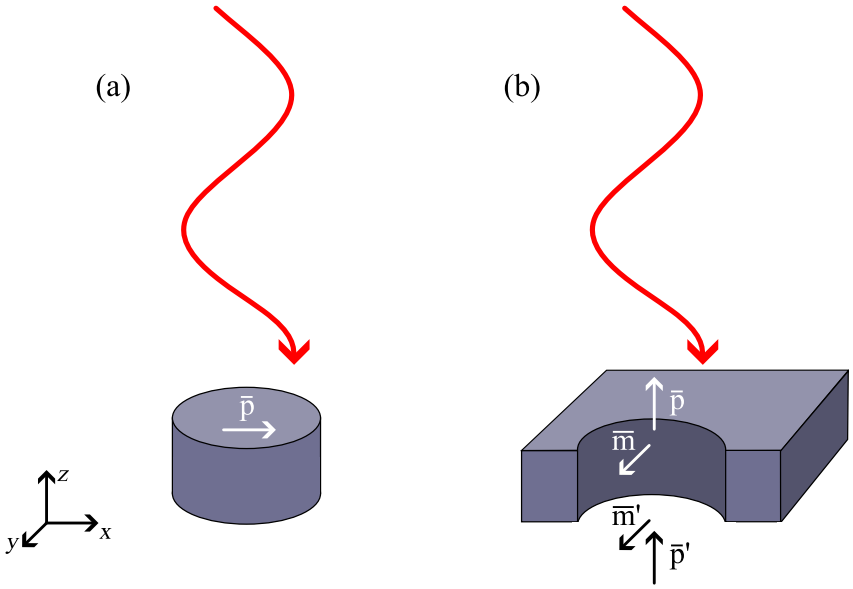

Figure 3.1. *A schematic picture of dipole moments in an individual particle and a hole. (a) shows the electric dipole moment induced in a nanoparticle and (b) shows the dipole moments in a hole. The dipole moments on top of the hole are different from the ones at the bottom of the hole. The incident light in both pictures is x-polarized.*

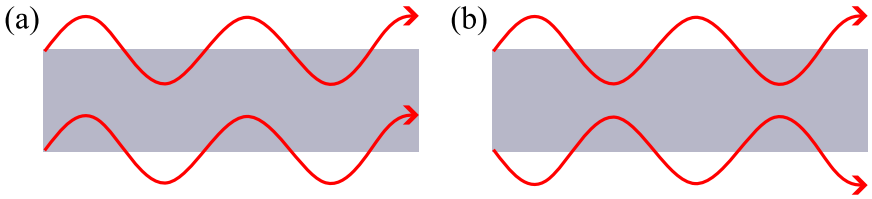

Figure 3.2. *The two different ways SPPs may propagate on the metallic film of a hole metasurface. In (a) the two SPPs on both sides of the metallic film have the same phase and in (b) they have the opposite phases.*

electromagnetic field components are the electric field components to x- and z-directions $\mathbf{E}_x$ and $\mathbf{E}_z$ and the magnetic field component to the y-direction $\mathbf{H}_y$ [6].

Metallic films have two sides on which the SPPs can propagate. The phase of these propagating SPPs can be the same on both sides of the film. However, hole arrays also allow the SPPs on the different sides to have opposite phases from each other [21]. This is schematically shown in Fig. 3.2.

3.3 Collective optical responses of periodic hole arrays

Holes in an array can couple to each other in the same way as particles can couple to one another in a particle array. These couplings result in SLRs which were introduced in the case of a particle array in Section 2.2. However, there is a major difference in the exact description of an SLR in a particle array and a hole array. In metallic particle arrays, we can usually ignore the coupling of magnetic dipoles since in metallic particles those are

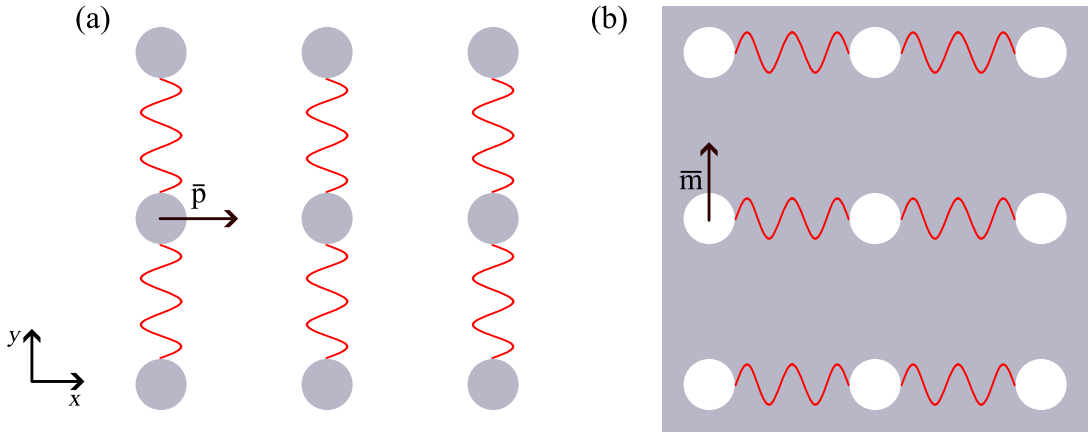

Figure 3.3. *(a) shows the coupling in a nanoparticle array. (b) shows the coupling in a hole array. The dipole moments determine the coupling direction since coupling cannot occur in a direction to which a dipole moment points. In both pictures, the incident light is x-polarized and travels along the normal of the metasurface plane.*

usually insignificant or nonexistent. This cannot be done in the case of a hole array.

The effects of magnetic coupling in hole arrays can be expressed using a lattice sum similar to Eq. (2.6). This sum affects both the electric and magnetic dipole moments on both sides of the metallic film. The exact equations for these effects are beyond the scope of this thesis. An interested reader is referred to section III of García de Abajo's review paper [8].

The coupling directions are different in hole arrays compared to particle arrays. This is illustrated in Fig. 3.3. Since coupling cannot occur to a direction a dipole moment points, for x-polarized light hole arrays couple in the x-direction while nanoparticle arrays couple in the y-direction. This means that in hole arrays changing the period in x-direction changes the SLR wavelength for x-polarized light.

4. BOUNDARY-ELEMENT METHOD SIMULATIONS USING COMSOL SOFTWARE

COMSOL Multiphysics is a simulation software for physics simulations. In this chapter, we will introduce how to use the software (version 6.1) to simulate optical phenomena in periodic metamaterials.

4.1 Creating a simulation model

When creating a new COMSOL model you can choose to either use *Model Wizard* or to create a completely blank model. The use of *Model Wizard* is advisable. After choosing to use *Model Wizard* one must choose the spacial dimensions of the simulation model and what kind of physics to simulate. In our case, we select our model to be in 3D, and for the physics we choose *Electromagnetic Waves, Frequency Domain* under *Wave Optics* which is under *Optics*. After this, one could select a *study*. However, we will leave introducing studies to Section 4.2.

A COMSOL model is built from many different features all of which have settings that define their location and behavior. The features are not only limited to the features defining the model's geometry but also include the more abstract features which describe all the relevant physics. An example of a COMSOL model and its different features can be seen in Fig. 4.1. In this Figure, the most relevant features are labeled with lowercase letters (a–l) both in *Model Builder* and in *Graphics*. These labels are added labels and are not part of the COMSOL software. Similar features are labeled with the same color. In *Model Builder*, the features are organized under sections that are labeled with maroon uppercase letters (A–F). These sections and the features underneath them will now be introduced in order.

(A) Parameters

In *parameters* section you can assign variable names to different parameters in the simulation. Even though one can build a simulation model without using parameters, using them makes it easier to modify the simulation. A parameter can be called anywhere in the model by simply typing its name into the expression where you want to use the param-

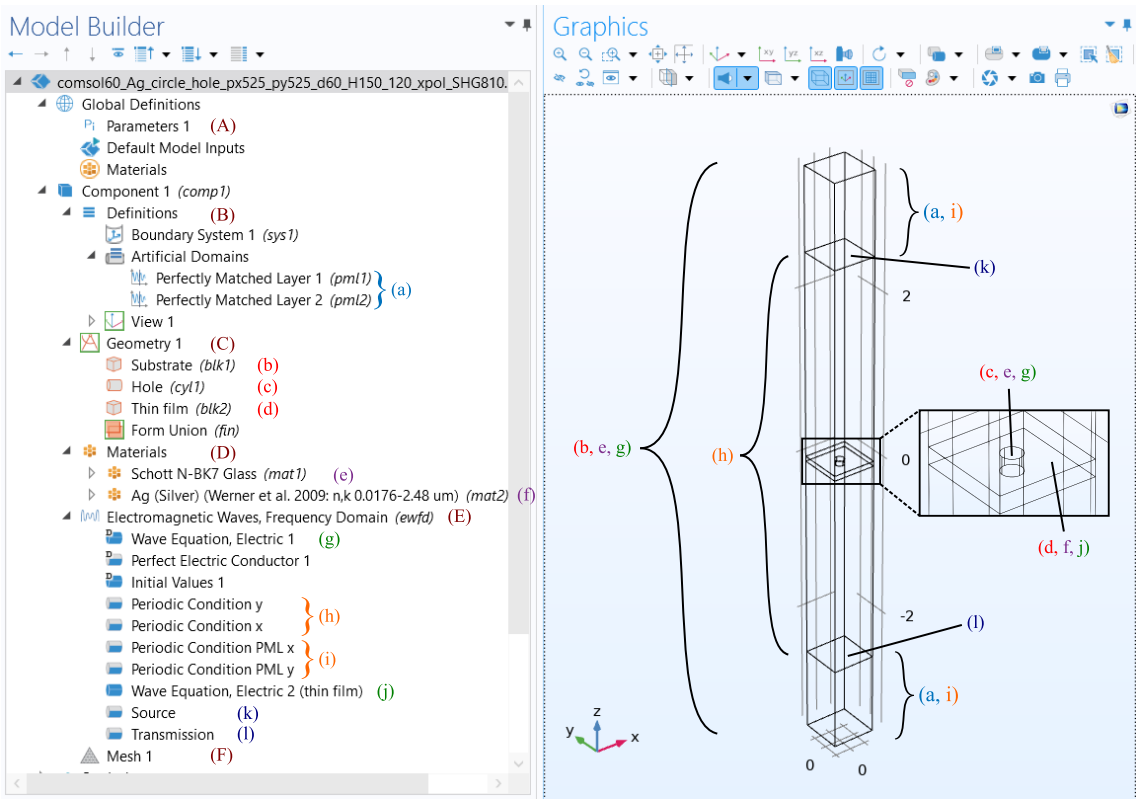

Figure 4.1. *A COMSOL model. The left side displays Model Builder where the features of the model are defined and the right side displays the model graphically. On the left letters (A–F) show the most important main sections of Model Builder. Letters (a–l) display features of the model in Model Builder and where those features are located graphically in the model. Similar features are labeled with the same color. Note that features (h, i, k, l) apply only to domain boundaries while all the other features apply to entire boundaries.*

eter's value. While use of parameters is often optional, this is not always the case. For example, *parametric sweeps* need a parameter to sweep over. Parametric sweeps are introduced further in Section 4.2. An example of a parameter table is shown in Fig. 4.2.

(B) Definitions

Definitions section contains among other things *local variables* and *selections*. For us the most relevant feature, however, is the *perfectly matched layer* (PML), labeled with (a) in Fig. 4.1.

PMLs are *artificial domains* that absorb light. They aim to enable light to exit the simulation volume with minimal effects on the actual simulation i.e. with minimal reflections. Therefore, they are needed for the top and bottom of the model from where most of the light is attempting to exit the simulation volume. Without PMLs, the light would reflect off the outer boundaries of the simulation volume. This would give rise to a new periodic response that is only present in the simulation and not in the actual fabricated sample. Therefore, one should avoid, or at least minimize, such unphysical responses. PMLs are

Name	Expression	Value	Description
d	20 [nm]	2E-8 m	Film thickness
px	522 [nm]	5.22E-7 m	x-periocity
py	522 [nm]	5.22E-7 m	y-periocity
z_span	5000 [nm]	5E-6 m	Simulation height
n_sub	1.51	1.51	Refractive index
d_pml	1000 [nm]	1E-6 m	PML height
phi	0 [deg]	0 rad	Pol angle, x is 0, y is 90
r	55[nm]	5.5E-8 m	circles radius

Figure 4.2. *A parameter table. The table consists of multiple parameters that all have a name, an expression and a value. The descriptions are voluntary.*

not the only way to let light escape the simulation volume. For example, *scattering boundary* conditions from the *physics* section can also sometimes be used. However, PMLs are often the best way to let the light escape since they reflect the least amount of light back and should therefore basically always be used at the top and the bottom of the simulation volume.

(C) Geometry

Geometry is the section where one can define the physical shape and dimensions of the simulation model. COMSOL offers some basic building blocks for building geometry as well as some more advanced tools.

In COMSOL, the basic building blocks can be found under *Primitives*. Primitives include some very simple shapes, for example, a *block*, a *cylinder* and a *sphere*. However, primitives also include some less basic geometric features like *Bézier curves*. In the model in Fig. 4.1 all of the geometry is built using primitives.

In the model mentioned above, (b) is the *block* that encompasses the whole simulation model. It defines three domains which are the PMLs at the top and the bottom of the model as well as the actual simulation volume. The separation into three domains is done using *layers* found in the settings of the *block*.

Features (c) and (d) define the geometries of the holes and the metallic film in which they reside. They are defined as a simple *cylinder* and a *block*, respectively. Note that the metallic film could have been built as a part of the (b) block using *layers* However, for the sake of conceptual clarity and in order to make the model more reconfigurable we chose to not use *layers*. For example, this way if we wished to remove the film, we'd only have to disable the (d) block from *Model Builder*.

More complicated structures, such as hole arrays with more arbitrarily shaped holes, can

also be constructed. This can be done for example by using a combination of *work planes* and *extrudes* as well as *booleans and partitions*. These are however beyond the scope of this introduction to COMSOL.

(D) Materials

In *Materials* section one can define the properties of materials composing the structure such as *refractive index* and *electrical conductivity*. However, materials do not define the physical behavior of the domain meaning that, for example, defining the metallic film to be silver doesn't automatically make the optical properties of silver follow the Drude model. That has to be done in *Physics* section.

COMSOL contains a vast library of materials from which to choose. If none of these materials work for you, you can always define a blank material and add *properties* to it. All domains, including *artificial domains* like PMLs, must have a material assigned to them. Those materials also must have all the *properties* needed for the physics simulation. This means that you often have to add properties to the materials even for materials from the material library.

(E) Physics

Physics sections are the sections where one can define the physics used to solve the model. A single model can have multiple different *physics* sections. However, we'll limit our scope to models with only one *physics* section and only to *Electromagnetic Waves, Frequency Domain* section. In Fig. 4.1 the most important *physics* features for simulating periodic metamaterials can be seen. Those are the *wave equations* (g, j), *periodic conditions* (h, i) and *ports* (k, l).

Wave equations define the light–matter interaction and the electric displacement field in a domain. Therefore, all domains must have a wave equation defined. In the example model, the electric displacement field of glass defined in (g) is simply defined by using the material's relative permittivity. However, the electric displacement field of silver is defined with the Drude–Lorentz dispersion model without any Lorentzian terms in (j).

The *periodic conditions* (h, i) make the simulation behave as if there were an infinite number of simulation volumes repeating along the direction of the periodic condition. This is achieved by making sure that the electromagnetic field at a point on a periodic condition is the same as the electromagnetic field at the corresponding point on the corresponding periodic condition. This way, a wave of light coming into contact with a periodic condition appears on the other side of the model like it would if there were another simulation volume there.

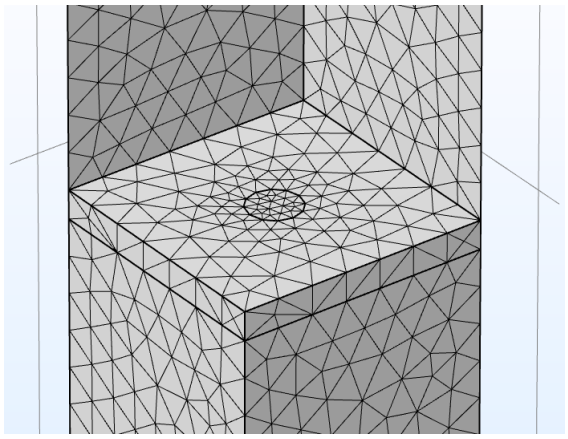

Figure 4.3. *A physics-controlled mesh. The hole can be seen in the picture as a circle with black edges. The hole can be detected because no cell in the mesh can be a part of two different domains and this makes the interfaces between two domains easy to spot. Also, we can see that the mesh is finer around the hole where the field can fluctuate more.*

Ports detect the light that travels through them. They can also be used as a light source. In the example model, port (k) acts as a detector and a light source. All of the light in the model originates from this port. It also measures how much light reflects from the metallic film. The (l) port at the bottom of the model only detects light. It measures the transmission of light through the metallic film.

(F) Mesh

In *Mesh* section one can define how the geometry of the model is divided into smaller pieces known as cells. This act of dividing the simulation volume is called *meshing* and the divided geometry is called a *mesh*.

When performing simulations, the electromagnetic field equations are solved in each cell and combined with the solutions from the other cells to form a solution for the entire simulation volume. An example of a mesh can be seen in Fig. 4.3.

The approximations within a cell have a simple mathematical form and therefore smaller cell sizes, i.e. finer meshes, give more degrees of freedom for the overall solution and are therefore more accurate. However, finer meshes are also computationally more demanding and therefore take more time.

In COMSOL, you can choose the mesh to be either a *user-controlled mesh* or a *physics-controlled mesh*. User-controlled meshes give more freedom to the user making it possible to customize the mesh for their structure. However, physics-controlled meshes are often good enough as long as the size of the cells is defined to be small enough.

4.2 Executing simulations and extracting results

In COMSOL, simulations are executed by using *studies*. Studies define the simulation and contain the results of the simulation. We will first introduce how to create a study and then explain how to extract the results from a study.

Creating a study

Studies are used for executing the simulations. They can be added during the creation of the model when using *Model Wizard* but also at any time from the *Study* tab. When adding a study you must choose a *study step*. Study steps define what a study simulates. All studies must have at least one study step but a study may also have many steps. There also exist many different types of study steps such as *Time Dependent*, *Eigenvalue* and *Wavelength Domain* study steps. Now we will proceed to take a closer look at the *Wavelength Domain* study step after which we will continue to *sweeps*.

Wavelength Domain takes a wavelength or wavelengths as an input and then executes a simulation on the model using those wavelengths. The ports working as light sources produce light with the frequency a light wave would have in a vacuum with the given wavelength. This study step can be used for calculating among other things the total electric and magnetic energies, the electromagnetic fields in the model and the total transmittance and total reflectance of the model.

Often a simulation must be computed many times with some small changes to the model to see how that affects the results. For example, one might want to know how the value of a certain parameter changes the results. These changes can be done by using *sweeps*. Some parameters don't affect the meshing of the model and can be "swept" over by using *auxiliary sweep* built in the *Wavelength Domain* study step. However, in a general case varying the value of a parameter or parameters can be done by using *parametric sweeps*.

Parametric sweeps take a parameter and its values as input and computes the study steps for each value which can be very useful. For example, parametric sweeps give us an efficient way to design and optimize the dimensions of the simulated device to get the desired response. Parametric sweeps can also sweep over multiple parameters simultaneously. There also exist other sweeps like the *material* and the *function sweeps*.

Extracting results from a study

After a study has been created and computed you can start handling the results of the simulation. COMSOL offers many ways to do this.

Perhaps the simplest way to view the results is by drawing plots within the COMSOL

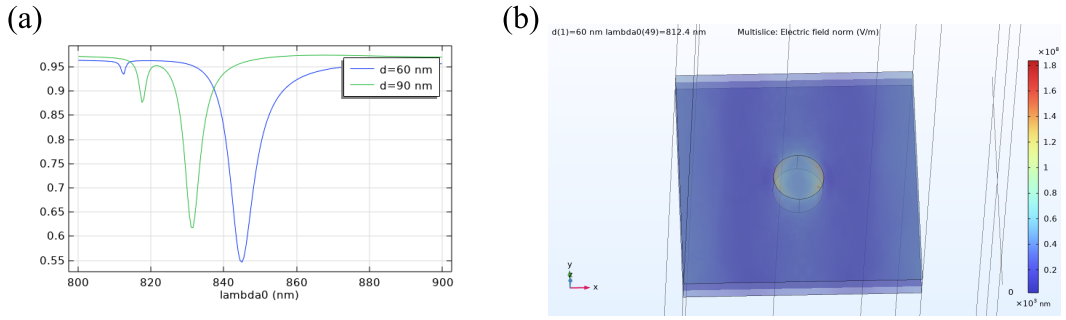

Figure 4.4. *Plots drawn in COMSOL. (a) is an example of a 1D plot and (b) is a 3D plot.*

software. These plots are quick to draw and informative. There is also many different kinds of plots like *1D*, *2D*, *3D* and *polar* plots. However, they might not look visually the best which is why these plots are rarely used in finished publications. These plots are still great for checking if your simulation produced sensible results or if your simulation model had a flaw in it. Examples of plots drawn using COMSOL can be seen in Fig. 4.4.

There are a few ways to extract result data from COMSOL to other pieces of software. One way is to create a table of the data and then copy that data to a spreadsheet. This is useful for results that can be plotted using the 1D plot. For example, extracting the total transmittance of your model can be done by creating a *Global Evaluation*, selecting the study and dataset of your results and defining the expression for the total transmittance. Now evaluating the *Global Evaluation* gives you a table that can be copied.

Another way to extract the results is to use the *export* feature of COMSOL and export the data to a new file. When using export you can define the points of the model from which to get the data. This way you can, for example, get the electric field inside the simulation volume.

5. RESULTS AND ANALYSIS

In this chapter, we will present the results of our simulations and analyze them. The simulations were performed on a nanoparticle array with cylinder shaped particles and to its complementary a hole array with circular holes. The simulations were done with particle height or film thickness of 60 nm and with periods to both x- and y-directions being 522 nm unless otherwise specified. Particle height and film thickness scans were done from 40 nm to 100 nm with 10 nm steps and periodicity scans were done from 514 nm to 530 nm with 4 nm steps. The material of the particles and the metallic film is silver and the dielectric substrate is *Schott N-BK7 Glass*. The periodicity scans were done with slightly different material properties of the *Schott N-BK7 Glass*. All simulations were done using x-polarized light.

5.1 Extinction spectra of nanoparticle and nanohole arrays

Extinction spectra of particle and hole arrays are presented in Fig. 5.1. Like Babinet's principle would suggest there are similarities in the spectra but there also are quite big differences. On the left at wavelengths around 600–650 nm both structures have an LSPR peak. However, the LSPR peak in hole arrays is much narrower than the LSPR peak in particle arrays. On the right at wavelengths little over 800 nm, we can see SLR peaks in both structures. The SLR peak in particle arrays is clearly more visible than the one in hole arrays. However, the most interesting result is that the hole array has another, less visible, SLR peak, noted by * in Fig. 5.1.

Quality factors (Q-factors), express the width of a resonance peak. Higher Q-factors mean longer resonance lifetimes and peaks with high Q-factors are better for many applications. Q-factors are calculated with the equation

$$Q = \frac{\lambda_0}{\Delta\lambda} \tag{5.1}$$

where λ_0 is the wavelength of the highest point of the peak and $\Delta\lambda$ is the line width of the peak. We fitted a curve to all the SLR peaks seen in Fig. 5.1 and calculated the Q-factors based on those fits. The fits are presented in Fig. 5.2.

The Q-factor of the SLR peak in the particle array is 110. The Q-factor of the more

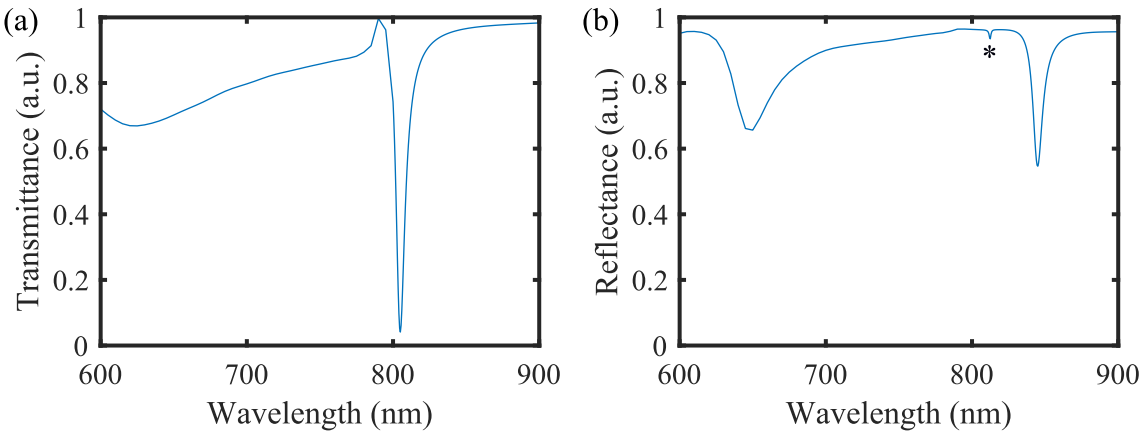

Figure 5.1. *Extinction spectra of particle and hole arrays. (a) shows the transmittance spectrum of a nanoparticle array and (b) the reflectance spectrum of the complementary hole array.*

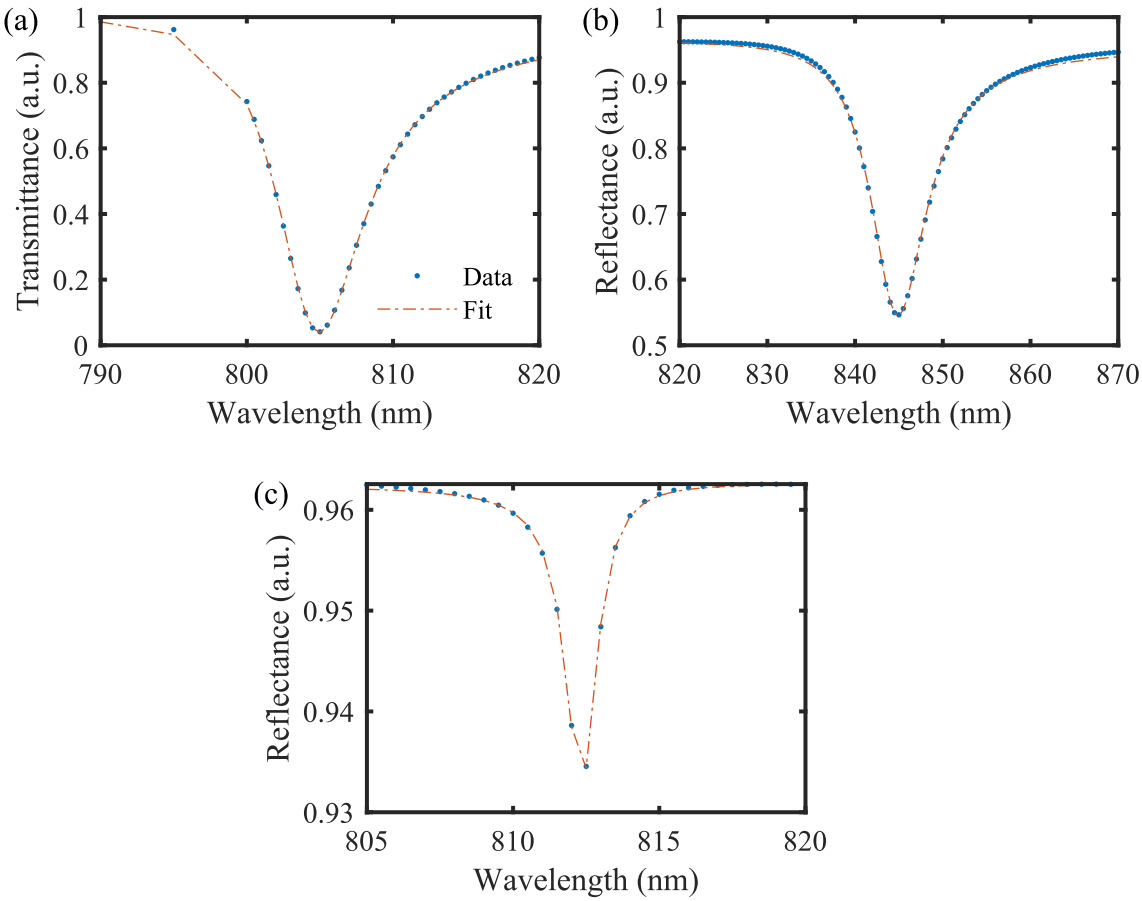

Figure 5.2. *Fits used to calculate the Q-factors of the SLR peaks. (a) shows the SLR peak for the nanoparticle array. (b) is the bigger SLR peak in the extinction spectrum of the hole array and c) is the less visible SLR peak seen in that spectrum.*

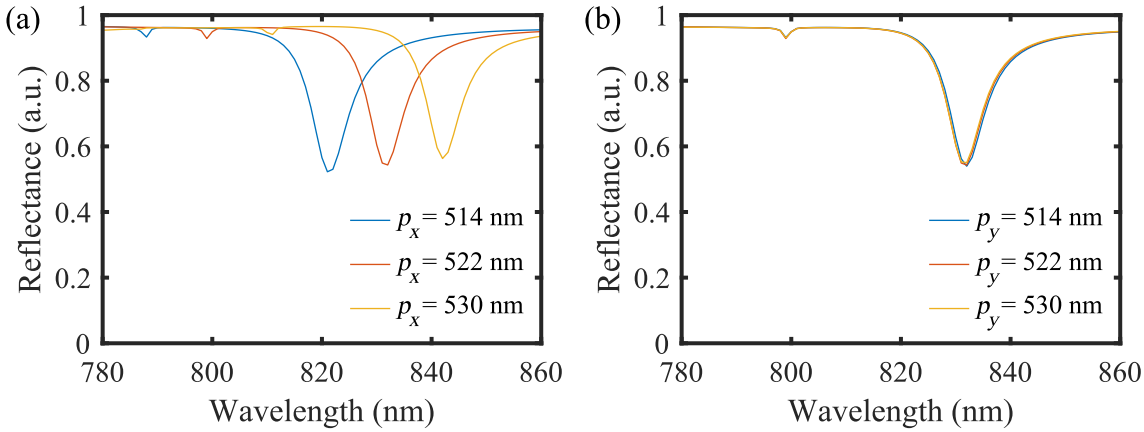

Figure 5.3. *The extinction spectra of the hole array with multiple different periods. (a) shows how the period in the x-direction p_x affects the SLR peaks. In (b) we can see that the period in the y-direction p_y doesn't affect the SLR peaks. The period to the direction not stated in the legend is 522 nm. These simulations used slightly different materials than the simulations in other sections and therefore these results cannot be directly compared to the results in other sections.*

visible SLR peak in the hole array is also 110. This suggests that even the SLRs of hole arrays with more visible peaks can be used in the same applications as SLRs of particle arrays. However, the Q-factor of the less visible SLR peak of the hole array is 608 which is considerably higher than the Q-factor of the SLR peak in the particle array.

5.2 Dependence of collective excitations on the period

All simulations in this section used slightly different materials than the simulations in other sections and therefore the results cannot be directly compared to the results in other sections.

As it was stated in Chapter 2, nanoparticles couple in y-direction when subjected to x-polarized light. The wavelengths of the SLRs resulting from these couplings are directly proportional to the period in the y-direction. For hole arrays, the period in the y-direction doesn't affect the SLR wavelength but the period in the x-direction does as can be seen in Fig. 5.3. These results show that the coupling in hole arrays is in the x-direction i.e. parallel to the polarization of incident light as was stated in Section 3.3.

The peaks of arrays with longer periods are a bit shallower than the peaks of arrays with shorter periods. This could be explained by the fact that the longer distance the SPPs have to travel the weaker they get and therefore the coupling is also weaker.

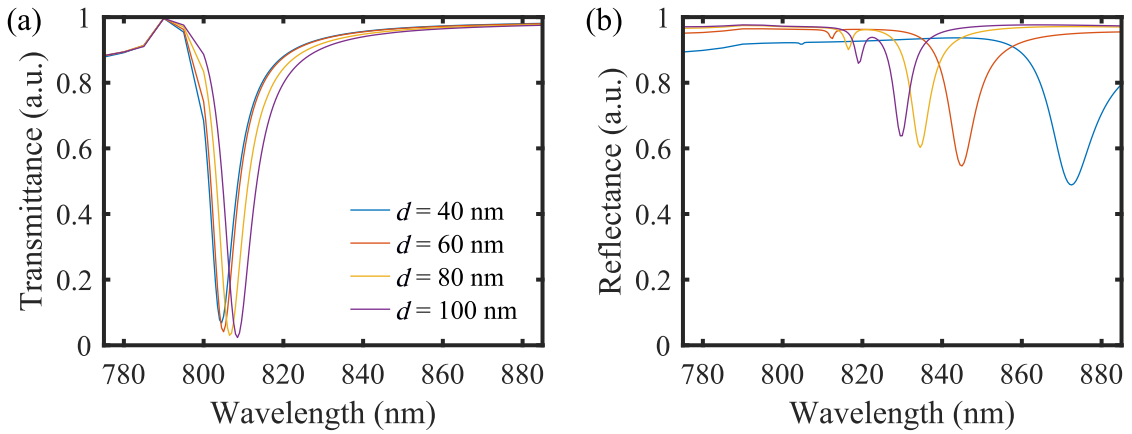

Figure 5.4. *The extinction spectra of particle and hole arrays with varying thicknesses of the metallic film in the collective response wavelength range. (a) shows the spectra for particle arrays and (b) for hole arrays.*

5.3 Dependence of collective excitations on the film thickness

In Fig. 5.4 simulated extinction spectra as functions of particle height and film thickness are presented. From (a) we can see that the SLR wavelength in nanoparticle arrays isn't much affected by the height of the nanoparticle. However, the thickness of the film in a hole array does affect the height of the SLR peaks as well as their position on the spectrum. For thinner films, the more visible SLR peak becomes deeper and moves towards longer wavelengths. On the other hand, the less visible SLR peak becomes shallower and moves towards shorter wavelengths.

We can calculate the Q-factors to the SLR peaks in films of varying thickness using the same method as in Section 5.1. These Q-factors are presented in Table 5.1. The Q-factor is the highest at the less visible peak in the thinnest film. However, Q-factors of the more visible peaks increase as the film thickness increases.

5.4 Calculated local-field distributions

The local-field distributions were calculated at the top and the bottom of the metallic film in order for us to explain the less visible SLR peak in the spectrum of the hole array. The normalized electric and magnetic field components at the top of metallic film at the SLR wavelength of the more visible SLR peak (845 nm) in a hole array are presented in Fig. 5.5.

In Fig. 5.5 we can see from components $\mathbf{E}_z$ and $\mathbf{H}_y$, and to a lesser extent from component $\mathbf{E}_x$, a sinusoidal wave to the x-direction. The maxima and minima of the $\mathbf{H}_y$ components occur at the zeros of the $\mathbf{E}_z$ component which suggest that the wave is a standing wave similar to one that occurs when light reflects off a mirror. This would mean that SPPs are traveling to both positive and negative x-direction. This clearly shows that

Table 5.1. *The SLR wavelengths and Q-factors of SLR peaks in hole arrays with varying film thicknesses.*

Type	Thickness (nm)	SLR wavelength (nm)	Q-factor
less visible peak	40	805	805
	50	809	739
	60	812	608
	70	815	487
	80	816	394
	90	818	337
	100	819	290
more visible peak	40	872	65
	50	855	89
	60	845	110
	70	839	135
	80	835	147
	90	831	161
	100	829	171

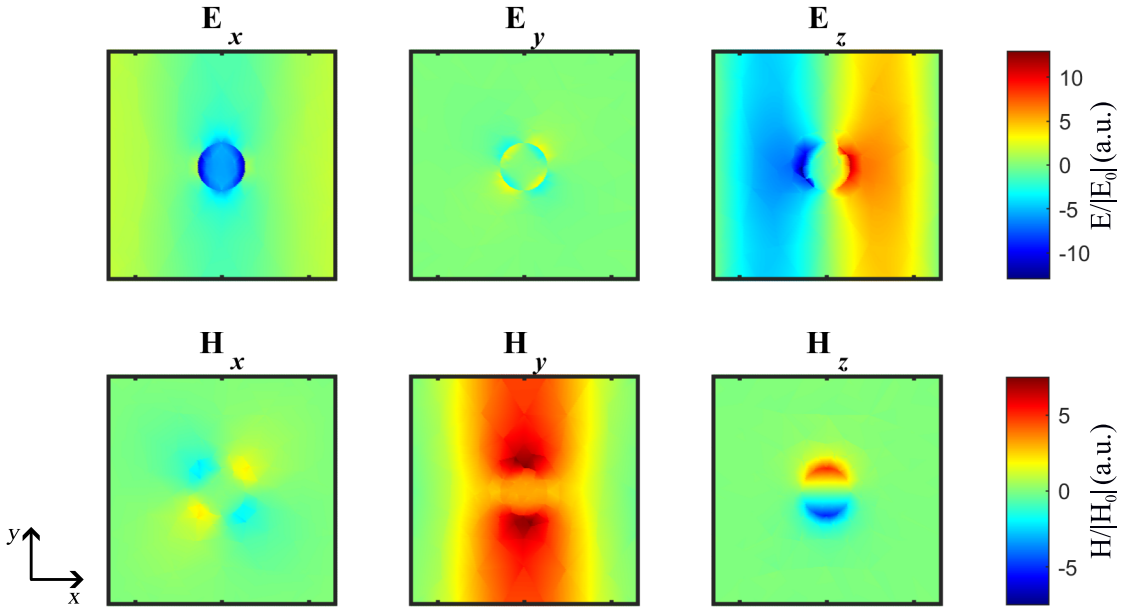

Figure 5.5. *Normalized electric and magnetic field components at the top of metallic film at SLR wavelength of the more visible SLR peak (845 nm) in a hole array.*

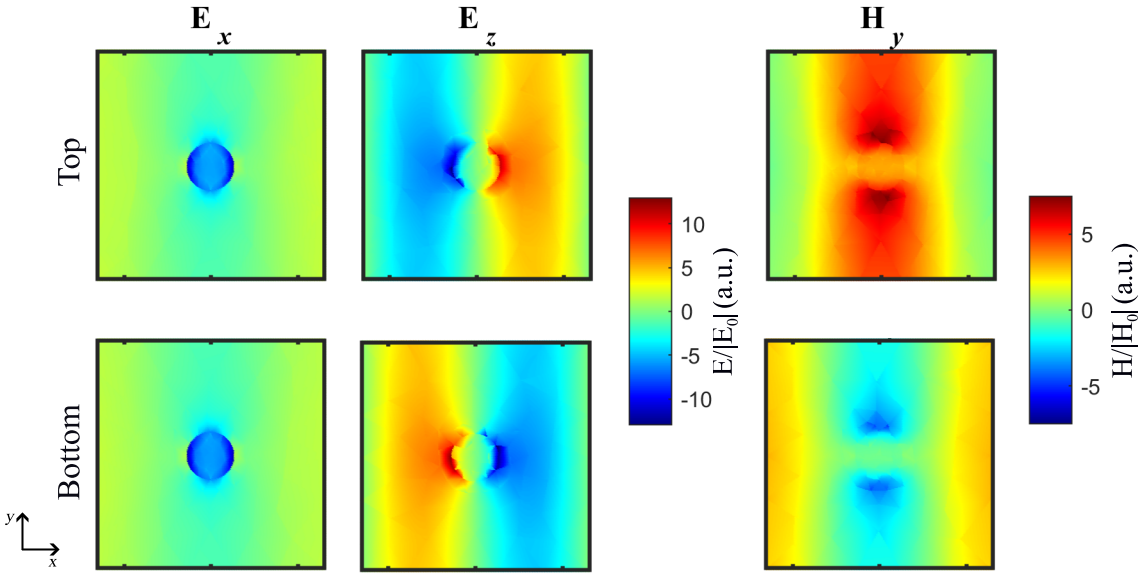

Figure 5.6. *Selected normalized electric and magnetic field components on top of the metallic film and at the bottom of the metallic film at the SLR wavelength of the more visible SLR peak (845 nm) in a hole array.*

the SPPs coupling the holes travel to the $\pm x$-directions which explains the shift of the SLR peaks shown in Section 5.2. We can also see that components $\mathbf{E}_y$, $\mathbf{H}_x$ and $\mathbf{H}_z$ are near zero except near the hole. This is to be expected since SPPs only exist for TM polarization as mentioned in Section 3.2. Therefore these fields will be disregarded from further analysis.

Fig. 5.6 shows the selected components of the electric and magnetic fields both at the top and at the bottom of the metallic film at the SLR wavelength of the more visible SLR peak (845 nm). Fig. 5.7 shows the corresponding fields at the SLR wavelength of the less visible SLR peak (812 nm).

Using Figs. 5.6 and 5.7, we can compare the electromagnetic fields which occur at the two SLR wavelengths. The first thing to notice is that the SPPs at the wavelengths of the more visible peak have a different phase at the top of the metallic film than at the bottom of the film corresponding to picture (b) in Fig. 3.2 and at the wavelengths of the less visible peak the SPPs have the same phase corresponding to picture (a) in the same figure. However, in the more visible peak, the $\mathbf{E}_x$ components have the same phase, while in the less visible peak, $\mathbf{E}_x$ components have opposite phases. $\mathbf{E}_x$ is an in-plane electric component and could radiate away energy from the metallic film in the case of the more visible peak. However, for the less visible peak, the opposite phases of the $\mathbf{E}_x$ components could lead to destructive interference which lessens this energy loss resulting in longer lifetimes and therefore higher Q-factors.

In the case of the more visible peak, we can see strong magnetic fields to the y-direction at the edges of the hole suggesting a strong magnetic dipole moment. These cannot

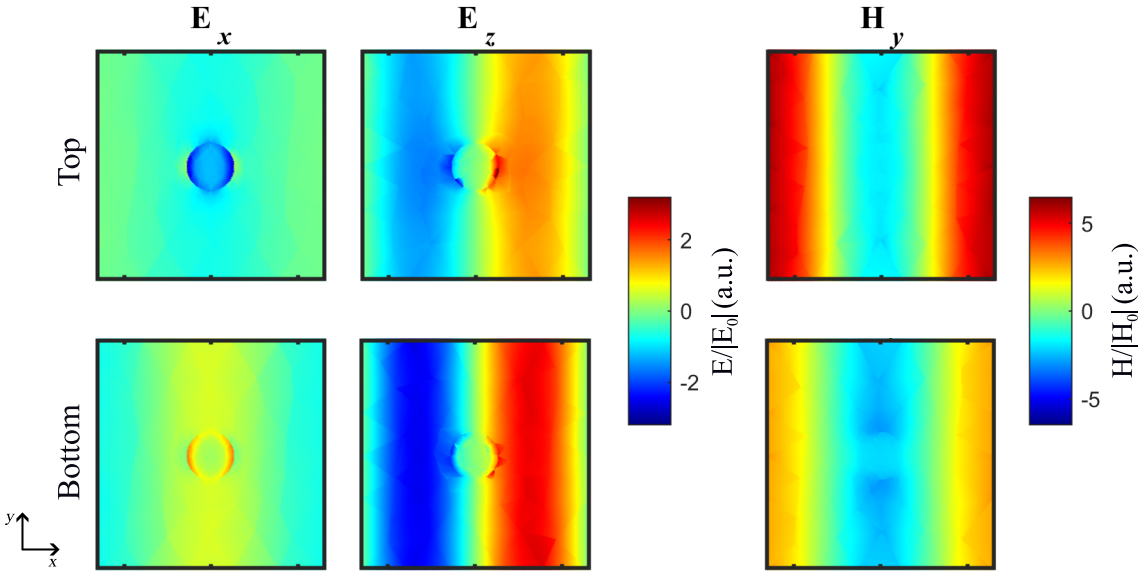

Figure 5.7. *Selected normalized electric and magnetic field components on top of the metallic film and at the bottom of the metallic film at the SLR wavelength of the less visible SLR peak (812 nm) in a hole array.*

be seen in the fields of the less visible peak. This could mean that the more visible SLR peak is due to magnetic coupling and the less visible SLR peak is due to electric coupling. Similar behavior has been observed in the case of dielectric particle arrays [22].

As a final observation, the electric field strength in the more visible peak is much higher than the electric field strength of the less visible peak. However, the magnetic field strengths are almost the same.

6. CONCLUSION

Hole arrays in metallic films have similar optical responses and resonances to nanoparticle arrays as expected by Babinet's principle. However, the responses can also have many differences between them.

SLRs occur in both nanoparticle and hole arrays. However, while particle arrays have only one SLR peak, hole arrays can have two. This second, less visible, SLR peak has a significantly higher Q-factor meaning that it has a longer resonance lifetime and is therefore promising for many applications such as enhancing non-linear optical effects. This longer lifetime may be caused by destructive interference in the hole which reduces radiation losses associated with the resonator.

The wavelength of the SLR depends on the periodicity of the metamaterial. Lattices with shorter periods in the coupling direction have shorter SLR wavelengths than lattices with longer periods in that direction. However, the direction of the period which affects the SLR wavelength in hole arrays is different from the direction of the period which affects the SLR wavelength in particle arrays. For x-polarized light the relevant period for particle arrays is the period to the y-direction. For hole arrays, it's the period to the x-direction. This difference in the coupling directions arises from the fact that in nanoparticle arrays, incident light polarized along x-direction mainly excites electric dipoles that point along x-direction. These electric dipoles subsequently scatter light dominantly along the y-direction. However, in hole arrays, x-polarized light excites magnetic dipoles in the y-direction which causes holes to scatter light dominantly along the x-direction.

The thickness of the metallic film of the hole array affects the SLRs. However, the corresponding parameter in particle arrays, the height of the particle, does not markedly affect the formation of SLRs. In hole arrays, thicker films lead to shorter SLR wavelengths, shallower peaks and higher Q-factors in the more visible SLR peak but to longer SLR wavelengths, higher peaks and lower Q-factors in the less visible peak.

The simulations were successful and they showed that hole arrays are a possible alternative to particle arrays and they could potentially be used in many of the same applications as particle arrays. The collective responses can be controlled by varying the parameters we researched here. However, the simulation results may have been more accurate with a finer mesh.

REFERENCES

[1] Overvig, A. C., Shrestha, S., Malek, S. C., Lu, M., Stein, A., Zheng, C. and Yu, N. Dielectric metasurfaces for complete and independent control of the optical amplitude and phase. *Light, science & applications* 8.1 (2019), p. 92. ISSN: 2047-7538. DOI: 10.1038/s41377-019-0201-7.

[2] Ye, W., Zeuner, F., Li, X., Reineke, B., He, S., Qiu, C.-W., Liu, J., Wang, Y., Zhang, S. and Zentgraf, T. Spin and wavelength multiplexed nonlinear metasurface holography. *Nature communications* 7.1 (2016), p. 11930. ISSN: 2041-1723. DOI: 10.1038/ncomms11930.

[3] Aieta, F., Genevet, P., Kats, M. A., Yu, N., Blanchard, R., Gaburro, Z. and Capasso, F. Aberration-Free Ultrathin Flat Lenses and Axicons at Telecom Wavelengths Based on Plasmonic Metasurfaces. *Nano letters* 12.9 (2012), pp. 4932–4936. ISSN: 1530-6984. DOI: 10.1021/nl302516v.

[4] Zhang, S., Kim, M.-H., Aieta, F., She, A., Mansuripur, T., Gabay, I., Khorasaninejad, M., Rousso, D., Wang, X., Troccoli, M., Yu, N. and Capasso, F. High efficiency near diffraction-limited mid-infrared flat lenses based on metasurface reflectarrays. *Optics express* 24.16 (2016), pp. 18024–18034. ISSN: 1094-4087. DOI: 10.1364/OE.24.018024.

[5] Stolt, T., Vesala, A., Rekola, H., Karvinen, P., Hakala, T. K. and Huttunen, M. J. Multiply-resonant second-harmonic generation using surface lattice resonances in aluminum metasurfaces. *Optics express* 30.3 (2022), pp. 3620–3631. ISSN: 1094-4087. DOI: 10.1364/OE.449198.

[6] Maier, S. A. *Plasmonics: Fundamentals and Applications*. 1st ed. 2007. Springer US, 2007. ISBN: 1-280-86588-1.

[7] Mochán, W. Plasmons. *Encyclopedia of Condensed Matter Physics*. Ed. by F. Bassani, G. L. Liedl and P. Wyder. Oxford: Elsevier, 2005, pp. 310–317. ISBN: 978-0-12-369401-0. DOI: https://doi.org/10.1016/B0-12-369401-9/00661-6.

[8] Abajo, F. G. de. Colloquium: Light scattering by particle and hole arrays. *Reviews of modern physics* 79.4 (2007), pp. 1267–1290. ISSN: 0034-6861. DOI: 10.1103/RevModPhys.79.1267.

[9] Hecht, E. *Optics*. Fifth edition. Harlow, Essex, England: Pearson Education, 2017. ISBN: 978-1-292-09693-3.

[10] Wang, L., Wang, Q., Wang, T.-Q., Zhao, W.-M., Yin, X.-Y., Jiang, J.-X. and Zhang, S.-S. Plasmonic crescent nanoarray-based surface lattice resonance sensor with

a high figure of merit. *Nanoscale* 14.16 (2022), pp. 6144–6151. ISSN: 2040-3364. DOI: 10.1039/d1nr08341d.

[11] Huttunen, M. J., Dolgaleva, K., Törmä, P. and Boyd, R. W. Ultra-strong polarization dependence of surface lattice resonances with out-of-plane plasmon oscillations. *Optics express* 24.25 (2016), pp. 28279–28289. ISSN: 1094-4087. DOI: 10.1364/OE.24.028279.

[12] Utyushev, A. D., Zakomirnyi, V. I. and Rasskazov, I. L. Collective lattice resonances: Plasmonics and beyond. *Reviews in physics* 6 (2021), p. 100051. ISSN: 2405-4283. DOI: 10.1016/j.revip.2021.100051.

[13] Cherqui, C., Bourgeois, M. R., Wang, D. and Schatz, G. C. Plasmonic Surface Lattice Resonances: Theory and Computation. *Accounts of chemical research* 52.9 (2019), pp. 2548–2558. ISSN: 0001-4842. DOI: 10.1021/acs.accounts.9b00312.

[14] Maß, T. W. W. and Taubner, T. Incident Angle-Tuning of Infrared Antenna Array Resonances for Molecular Sensing. *ACS photonics* 2.10 (2015), pp. 1498–1504. ISSN: 2330-4022. DOI: 10.1021/acsphotonics.5b00399.

[15] Horák, M., Křápek, V., Hrtoň, M., Konečná, A., Ligmajer, F., Stöger-Pollach, M., Šamořil, T., Paták, A., Édes, Z., Metelka, O., Babocký, J. and Šikola, T. Limits of Babinet's principle for solid and hollow plasmonic antennas. *Scientific reports* 9.1 (2019), p. 4004. ISSN: 2045-2322. DOI: 10.1038/s41598-019-40500-1.

[16] Born, M. and Wolf, E. *Principles of Optics: Electromagnetic Theory of Propagation, Interference and Diffraction of Light*. Saint Louis: Elsevier Science & Technology, 1980. ISBN: 9780080264820.

[17] Bethe, H. A. Theory of Diffraction by Small Holes. *Physical review* 66.7-8 (1944), pp. 163–182. ISSN: 0031-899X. DOI: 10.1103/PhysRev.66.163.

[18] Jackson, J. D. *Classical electrodynamics*. 2. ed. New York: Wiley, 1975. ISBN: 0-471-43132-X.

[19] Thompson, P. G., Biris, C. G., Osley, E. J., Gaathon, O., Osgood, R. M., Panoiu, N. C. and Warburton, P. A. Polarization-induced tunability of localized surface plasmon resonances in arrays of sub-wavelength cruciform apertures. *Optics express* 19.25 (2011), pp. 25035–25047. ISSN: 1094-4087. DOI: 10.1364/OE.19.025035.

[20] Degiron, A., Lezec, H., Yamamoto, N. and Ebbesen, T. Optical transmission properties of a single subwavelength aperture in a real metal. *Optics communications* 239.1 (2004), pp. 61–66. ISSN: 0030-4018. DOI: 10.1016/j.optcom.2004.05.058.

[21] Berini, P. Long-range surface plasmon polaritons. *Advances in optics and photonics* 1.3 (2009), pp. 484–588. ISSN: 1943-8206. DOI: 10.1364/AOP.1.000484.

[22] Castellanos, G. W., Bai, P. and Gómez Rivas, J. Lattice resonances in dielectric metasurfaces. *Journal of applied physics* 125.21 (2019), p. 213105. ISSN: 0021-8979. DOI: 10.1063/1.5094122.